Experimental Study of Fibrin/Fibrin-Specific Molecular Interactions Using a Sphere/Plane Adhesion Model

Sylvie Lorthois,*,[1] Philippe Schmitz,* and Eduardo Anglés-Cano†

*Institut de Mécanique des Fluides de Toulouse, UMR CNRS 5502, Allée du Professeur C. Soula, 31400 Toulouse, France; and †INSERM U460 "Remodelage Cardiovasculaire," 16 Rue H. Huchard, BP416, 75870 Paris Cedex, France

Fibrin, the biopolymer produced in the final step of the coagulation cascade, is involved in the resistance of arterial thrombi to fragmentation under shear flow. However, the nature and strength of specific interactions between fibrin monomers are unknown. Thus, the shear-induced detachment of spherical monodispersed fibrin-coated latex particles in adhesive contact with a plane fibrin-coated glass surface has been experimentally studied, using an especially designed shear stress flow chamber. A complete series of experiments for measuring the shear stress necessary to release individual particles under various conditions (various number of fibrin layers involved in the adhesive contact, absence or presence of plasmin, the main physiological fibrinolytic enzyme) has been performed. The nonspecific DLVO interactions have been shown to be negligible compared to the interactions between fibrin monomers. A simple adhesion model based on the balance of forces and torque on particles, assuming an elastic behavior of the fibrin polymer bonds, to analyze the experimental data in terms of elastic force at rupture of an elementary intermonomeric fibrin bond has been used. The results suggested that this force (of order 400 pN) is an intrinsic quantity, independent of the number of fibrin layers involved in the adhesive contact.

Key Words: **particle adhesion; hydrodynamic detachment; fibrin; shear; bioadhesion; embolism.**

1. INTRODUCTION

Fragmentation of an arterial thrombus may lead to the phenomenon of embolization, i.e., the occlusion of distal smaller vessels by the fragments produced. The clinical consequences are serious and often fatal: heart attack, stroke, etc., depending on the location of the obstructed vessel. The main constituents of arterial thrombi are platelets and fibrin, the biopolymer produced in the final steps of the coagulation cascade. In this process, the thrombin-catalyzed conversion of soluble fibrinogen into insoluble fibrin monomers is followed by a noncovalent self-assembly of monomeric fibrin units into a three-dimensional meshwork (1), and platelets form anchoring points for fibrin fiber formation (2). This meshwork provides the structural support for arterial thrombi and appears to be the major constituent that controls their stability (1, 3, 4).

Thrombi fragmentation is mainly triggered by complex biochemical phenomenon and by the external mechanical loads exerted by the blood flow, especially the shear stress (4–8). However, the fundamental underlying mechanisms are still poorly understood. In particular, the nature and strength of the fibrin adhesive bonds holding platelets to each other, and the related resistance to external mechanical loads tending to break up these bonds, which are central issues related to arterial thrombi fragmentation, are still unknown.

For 15 years, considerable attention has been devoted to the relationship between biochemical and mechanical factors in the process of thrombi formation, using native or anticoagulated blood flowing over prothrombotic surfaces in shear stress flow chambers (5, 9–14). The results of these studies have demonstrated that thrombi composition, size, and structure, which probably influence the fragmentation process, are highly dependent on (a) the composition of the prothrombotic surface and (b) the wall shear stress.

In contrast, only a few studies on the problem of fragmentation have been done. In fact, this problem is very complex since fragmentation at least involves the numberous parameters also involved in thrombi formation and is the result of the collective behavior of numerous platelets entrapped into the fibrin meshwork and submitted to the shear flow action. Several experimental difficulties arise from this collective behavior (5, 8, 15): first, the modification of the thrombus macroscopic shape during its fragmentation modulates the shearing action of the blood flow, which precludes the experimental ability to control the shear stress; second it is difficult to dissociate the formation and the fragmentation phases, which may overlap in time.

Although the collective behavior of the platelets is probably different from the behavior of individual platelets in contact with a flat substrate, the mechanisms of individual platelet removal must be a key to understanding and analyzing the macroscopic fragmentation of an arterial thrombus. This simplified approach

[1] To whom correspondence should be addressed at current address: Department of Mechanical Engineering, University of California—Berkeley, 6195 Etcheverry Hall, Berkeley, CA 94720-1740. E-mail: lorthois@imft.fr.

has been followed recently by three different teams (16–18). However, their studies have been focused mainly on biochemical aspects. Due to the deformability and to the specific behavior of blood platelets (i.e., transition from a rest state to an activated state with activation of membrane receptors, release of active proteins, and shape change), a lot of parameters were very difficult to control and to modulate individually. Thus, there was no attempt to quantify the strength of the adhesive bond holding platelets to the flat substrate, and the results remained mainly qualitative.

By contrast, the aim of the present study was to gain quantitative insight on specific molecular interactions between fibrin monomers. For that purpose, a particular effort was made to individually control all experimental parameters. The fibrin meshwork studied was thus prepared under controlled biochemical conditions, i.e., under purified and static conditions. The blood platelets were modeled by 2-μm-diameter fibrin-coated spherical and rigid particles. These model particles were put in adhesive contact with a fibrin-coated glass plate, allowing fibrin/fibrin specific interactions to spontaneously form between the surfaces. This approach, where blood cells are replaced by coated spherical and rigid particles, to quantify the adhesion strength due to receptor/ligand interactions has been successfully used previously (19, 20). In addition, the shear stress flow chamber was carefully designed to give a fully developed laminar two-dimensional Poiseuille flow, resulting in the accurate knowledge of hydrodynamic forces and torque acting on individual particles.

A complete series of experiments for measuring the shear stress necessary to release individual particles under various conditions (various number of fibrin layers involved in the adhesive contact, absence or presence of plasmin, the main physiological fibrinolytic enzyme) was performed.

A simple adhesion model based on the assumption of an elastic behavior of the fibrin polymer bonds was developed in order to provide a useful basis to analyze the effects of the different parameters on the detachment mechanisms. It was used to analyze the experimental data in terms of elastic force at rupture of an elementary intermonomeric fibrin bond.

2. MATERIALS AND METHODS

2.1. Experiments

2.1.1. Preparation of the Immobilized Fibrin Meshwork

Reagents and particles. Reagents were purchased as indicated: 3-aminopropyl-diethoxymethylsiline (3-APDEMSilane) from ABCR (Kalsruhe, Germany); human thrombin from Diagnostica Stago (Asnieres, France); bovine serum albumin (BSA) from Eurobio (Les Ulis, France); glutaraldehyde, 25% (v/v) aqueous solution from TAAB Laboratories (Reading, UK); dansylphenylalanyl-L-propyl-L-arginine chloromethyl ketone (PPACK) from Biochem (Meudon, France). The monoclonal antibody Y18 was kindly provided by Dr. Nieuwenhuizen (Gaubius Laboratory, Leiden). All other reagents were of the best reagent grade commercially available.

Fibrinogen was purified from fresh-frozen human plasma as previously described (21) with modifications by Grailhe *et al.* (22). The purified fibrinogen was free of von Willebrand factor, plasminogen, plasmin, fibronectin, and factor XIII as determined by an enzyme-linked immunosorbent assay specific for these proteins. Fibrinogen was more than 98% clottable and the integrity of its three chains was checked by SDS–polyacrylamide gel electrophoresis of the reduced molecule. Protein concentration was determined by measuring the absorbance at 280 nm using $E^{1\%}_{1\mathrm{cm}} = 15.1$ (23).

Plasminogen was purified as previously described (24) from fresh-frozen human plasma. The purified plasminogen was free of plasmin as determined by an enzyme-linked immunosorbent assay specific for this protein. Protein concentration was determined by measuring the absorbance at 280 nm using $E^{1\%}_{1\mathrm{cm}} = 16.8$ (25). Plasmin was prepared by activation of purified plasminogen by urokinase immobilized on sepharose 4B (26).

Sulfate and amine latex particles stored in distilled and desionized water respectively containing 0 and 0.1% (v/v) sodium azide were from the Interfacial Dynamics Corporation (Portland, OR). According to the manufacturer, their diameters respectively were 2.1 μm $\pm$ 6.1% and 2.1 μm $\pm$ 3.4%. Their young modulus was 3 GPa and their density 1.055 g/cm^3.

Amino-modified glass surfaces. Amino-modified glass surfaces were prepared according to the procedure of Ho Moon *et al.* (27) with minor modifications. Briefly, $210 \times 90 \times 4$ mm^3 glass plates (Planilux Saint Gobain, France) were first incubated in a H_2SO_4, H_2O_2 30%, 7 : 3 (v/v) solution for 1 h, rinsed 10 times in distilled water, incubated in acetone for 3 min and dried at 110°C for 30 min. The cleaned surfaces were immersed into a 1% 3-APDEMSilane in anhydrous toluene (v/v) for 1 h and rinsed three times in toluene under a nitrogen atmosphere. Subsequently the slides were dried for 30 min at 120°C and incubated in toluene, a mixture of toluene and methanol (1 : 1, v/v), and methanol. Finally, the amino-modified glass slides were dried overnight at 120°C, and immediately used as support for fibrinogen immobilization.

As a control, AFM pictures of the cleaned and amino-modified glass surfaces were obtained using a Nanoscope II (Digital Instruments, Santa Barbara, CA) operated in "repulsive" mode (28) in 0.01 M sodium phosphate buffer, pH 7.4, containing 0.02 M NaCl and 0.01% (v/v) NaN_3. The measured RMS roughnesses of the cleaned and amino-modified glass surfaces, independent of the size of the scanning area, was respectively 0.249 ± 0.061 and 0.408 ± 0.115 nm, showing that the cleaning process was efficient for removing contaminating submicrometric particles without destroying glass surface integrity.

Preparation of fibrin monolayers. Solid-phase fibrin monolayers were prepared on amine latex particles and amino-modified glass plates as previously described (25, 29). Briefly, both types of support were first activated with a 2.5% (v/v)

poly(glutaraldehyde) solution in 0.1 M sodium bicarbonate buffer, pH 9.5, for 2 h at 37°C.[2] After washing the surface with distilled water, fibrinogen (100 μg/ml in 0.1 M sodium phosphate buffer, pH 7.4, containing 1 mM $CaCl_2$) was covalently immobilized by incubation for 18 h at 4°C. Unreacted fibrinogen was discarded, free aldehyde groups were neutralized by incubation with a 0.3 M solution of ethanolamine, pH 7.4, and the surface was finally rinsed three times with buffer A (0.05 M sodium phosphate buffer, pH 7.4, containing 0.08 M NaCl and 0.01% (v/v) NaN_3). The immobilized fibrinogen monolayer was transformed into a fibrin surface by treatment with thrombin (20 NIH units/ml in buffer A containing 1 mM $CaCl_2$) at 37°C for 2.5 h. Excess thrombin was eluted, and the fibrin monolayers were stored at 4°C in buffer A containing 20 mM L-Lysine and 5 mM PPACK.

The transformation of fibrinogen into fibrin upon treatment with increasing quantities of thrombin was demonstrated by the disappearance of immunoreactivity of the monoclonal antibody Y18, which recognizes an epitope situated in fibrinopeptide A released by thrombin. The subsequent spontaneous polymerization of fibrin monomers was demonstrated by the large increase of immunoreactivity of the monoclonal antibody DD3B6 (Agen Biomedical Ltd, Brisbane, Australia) upon treatment of fibrin monolayers with increasing quantities of plasmin. This antibody recognizes specifically an epitope present in fibrin D-dimers, the degradation product of polymerized fibrin, which is absent in fibrinogen and its degradation products. Therefore, immobilized fibrin has adopted the structure of a network of polymerized fibrin, rather than the structure of isolated monomers. In addition, the fibrin monolayers were able to bind tissue plasminogen activator (t-PA) and plasminogen with high affinity following the Langmuir theoretical predictions, and to subsequently catalyze plasmin formation, demonstrating that fibrin functionality was not impaired by the immobilization procedure.

AFM pictures obtained under the same conditions as described above showed that glutaraldehyde and fibrinogen were firmly fixed at the glass surface, indicating a success of fibrinogen grafting (30). In fact, whatever the number of scans, the tip was unable to remove glutaraldehyde and fibrinogen and the images remained identical, in contrast to images obtained after nonspecific physisorption of fibrinogen (31, 32). RMS roughness of the fibrin monolayer, independent of the size of the scanning area, was 2.342 ± 0.551 nm. This roughness, as well as the maximal amplitude of the image (21.17 ± 7.682 nm), was negligible compared to the radius of the latex particles.

Preparation of fibrin bilayers. Fibrin bilayers were prepared by incubating for 18 h at 4°C, 3 μM fibrinogen in 0.1 M sodium phosphate buffer, pH 7.4, containing 1 mM $CaCl_2$, with fibrin monolayers previously washed with buffer A containing 1 μM PPACK. After three washes with buffer A, fibrinogen thus bound was transformed into fibrin by treatment with thrombin (1 NIH unit/ml in buffer A containing 1 mM $CaCl_2$) at 37°C for 1 h. Excess thrombin was eluted and the fibrin bilayers were stored at 4°C in buffer A containing 20 mM L-lysine and 5 μM PPACK.

Transformation of fibrinogen into fibrin and subsequent fibrin spontaneous polymerization were demonstrated as described above.

2.1.2. Shear Stress Flow Chamber

The shear stress flow chamber was derived from the chamber of Elzo *et al*. successfully used to characterize particle/membrane interactions during a crossflow microfiltration process (33). The chamber was composed of a bottom glass plate ($210 \times 90 \times 4$ mm^3) onto which was prepared the immobilized fibrin meshwork, an upper Plexiglas plate ($210 \times 90 \times 10$ mm^3), and a hollwed stainless steel shim ($210 \times 90 \times 0.2 \pm 0.002$ mm^3) for channeling the fluid flow. All the plates were held together with aluminium clamps.

The fluid enters the chamber through a 1-mm-wide slit pierced perpendicularly in the upper plate. The slit follows a cylindrical compartment topped by a purge for removing air bubbles trapped in the fluid. The fluid exits the chamber through a 2-mm-diameter hole. A third orifice (0.26 mm diameter) topped by a syringe valve (Mininert VICI, Houston, TX) was used to inject the solution of latex particles. The shim hollowed area, the dimensions of which are given in Table 1, was cut up using a numerical milling machine (Atelier de Précision Mécanique, Blagnac, France).

The existence of a laminar unidirectional Poiseuille flow in the rectangular flow channel was demonstrated by experimental verifications of the theoretical relationship between pressure drop (ΔP) and flow rate (Q) for plane two-dimensional Poiseuille flows (34), showing the nondeformation of the flow chamber even at higher pressures applied. For this type of flow, the wall shear stress τ_w is uniform except in the boundary layers (width of order h) near the channel side walls and in a short entry region whose length L_e is about

$$L_e = 0.273\, h \mathrm{Re}_h, \qquad [1]$$

TABLE 1
Shear Stress Flow Chamber: Dimensions of the Hollowed Area in the Stainless Steel Plate, Which Delimitates the Flow Channel

	Length (mm)	Inlet width (mm)	Outlet width (mm)
Diverging channel	40	10	20
Converging channel	20	20	10
Rectangular flow channel	50	10	10
Outlet converging channel	10	10	5

Note. The rectangular flow channel follows a diverging-converging channel, in order to ensure a uniform flow at its entrance.

[2] A 3.14-mm^2 area was isolated on the glass plate using silicon press clip incubation chambers (Sigma, Saint Louis, MO). Amine latex particles were centrifuged for 5 min at 5000 rpm after each incubation and wash, the supernatant was discarded, and the pellet was redispersed in solution as described in text.

where h is the flow channel half-thickness and Re_h is the Reynolds number based on h and on the mean flow velocity. Outside, τ_w is given by

$$\tau_w = \frac{3\mu Q}{4h^2 l}, \qquad [2]$$

where μ is the dynamic viscosity of the fluid and l is the flow channel half-width.

2.1.3. Detachment Experiments

To start an experiment, the bottom glass plate of the chamber was coated with fibrin, then the chamber was assembled and placed on the stage of an inverted phase contrast microscope (Nikon Diaphot TDM, Tokyo, Japan). Unless otherwise stated, the flow chamber was filled with detachment buffer (sodium phosphate 0.05 M, pH 7.4, NaCl 0.08 M, NaN_3 0.01%). Fibrin-coated latex beads (10^7 beads/ml in detachment buffer) were slowly injected into the flow chamber through a syringe valve, and were allowed to settle under gravity for 2 h, resulting in bead separation distances between 5 and 10 bead diameters. This separation distance was chosen to minimize artifacts caused by interactions between particles, such as shielding of the shear field (35). Then the beads were incubated with the coated surface for 2 subsequent hours. After that time, the flow rate in the flow channel was increased step by step (a typical step was 3 min (34)). Flow rates ranging from 1 through 4.5 ml/min were generated by gravity, controlling the height of a constant head vessel located upstream of the chamber. Flow rates greater than 4.5 ml/min were obtained using a gear pump (Micropump, Vancouver, WA). At the end of each flow rate step, the number of particles remaining at the glass surface was counted by means of phase contrast optical microscopy and image acquisition/treatment. The shear stress applied was calculated using Eq. [2] from the value of flow rate measured by weighting on an electronic balance.

At the end of each experiment, the bottom fibrin-coated glass plate was stored and the fibrin presence was checked: the immunoreactivity of a sheep serum recognizing fibrinogen and fibrin was comparable for plates used in the detachment experiments and a control plate prepared simultaneously but not used in the detachment experiments, indicating that the fibrin layers have not been peeled away due to the flow shearing action.

In order to study the influence of fibrin degradation by plasmin, the following modifications were introduced. Before assembly of the flow chamber, the fibrin-coated glass plate was incubated for 14 h at 4°C with detachment buffer containing 1 μM plasminogen. Concurrently, fibrin-coated latex beads (10^7 beads/ml) were incubated for 14 h at 4°C in detachment buffer containing 50 U/ml t-PA. After that time, excess plasminogen was discarded by three washes of the glass plates in detachment buffer, and the chamber was assembled and filled with detachment buffer. Injecting the fibrin-coated latex bead solution containing t-PA triggered transformation of plasminogen bound to the fibrin-coated glass plate into plasmin, and subsequent degradation of the fibrin network.

At the end of each experiment, the bottom plasmin-degraded fibrin-coated glass plate was stored and fibrin degradation was checked: the increase of immunoreactivity of the monoclonal antibody DDi2F7 (Serbio, Asnières, France), which specifically recognizes fibrin degradation products, for plates used in the detachment experiments compared to a control plate prepared simultaneously but not used in the detachment experiments demonstrated a successful plasmin degradation during the course of the experiments.

2.1.4. Data Analysis

The number of particles initially present in the observation area was typically between 40 and 200. Thus, the representativity of each experiment was assessed using the methodology described previously (34). If not representative, the experiment was discarded. When applicable, experimental data were fitted to equations described in text. The best values for the parameters were determined using a least-squares regression method. Traditional formulas for the mean and the standard deviation (36) were used and are reported as mean value $\pm$ standard deviation. Independent sets of experiments (i.e., sets of experiments performed using fibrin-coated surfaces prepared independently) were compared for statistically significant differences using an unequal variance Student's t-test (36). Significant difference was denoted by $p < 0.05$.

2.2. Theoretical Framework

2.2.1. Relationship between Adhesion Force and Wall Shear Stress at Detachment

In order to interpret the experimental results, which describe the particle detachment as a function of the wall shear stress applied, the relationship between adhesion force and wall shear stress at detachment must be elucidated. One of the most important and sensitive parameter in this relationship is the radius of the contact area between particles and flat surface. When there are no specific interactions between the adhering surfaces, this contact area may be related to the microroughness or to the elastic and adhesive deformation of the surfaces (37–39). In our particular case, the presence of specific bonds between particles and surfaces defines the contact area, i.e., the area where such bonds are present (19, 40, 20). Assuming that the characteristic height of the surface roughness is small compared to the characteristic thickness of the fibrin meshwork binding the particle to the flat surface, as suggested by AFM observations, we have (see Fig. 1)

$$r_\mathrm{p}^2 = a^2 + (r_\mathrm{p} - l_0)^2, \qquad [3]$$

where r_p and a are the particle and the contact area radii, respectively, and l_0 is the characteristic thickness of the fibrin meshwork binding the particle to the flat surface. As l_0 is negligible

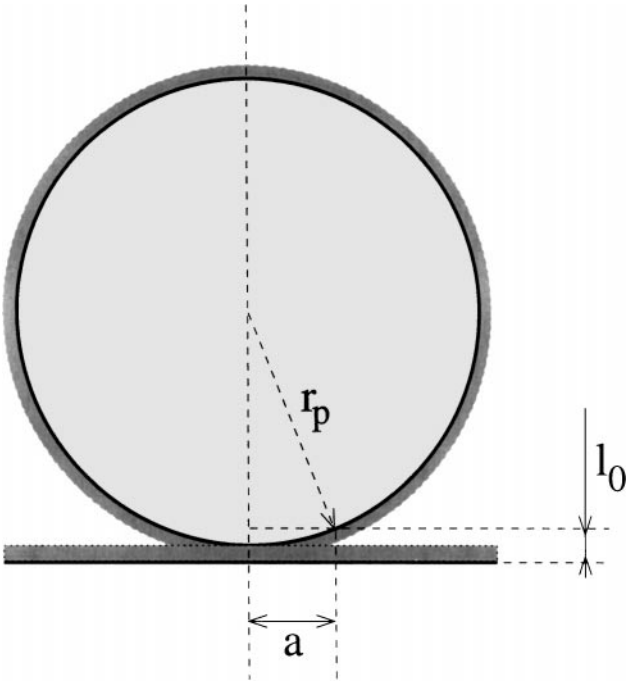

FIG. 1. Schematic diagram (not to scale) of a particle in contact with the flat surface. r_p and a are the particle and the contact area radii, respectively, and l_0 is the characteristic thickness of the fibrin meshwork (represented in gray) binding the particle to the flat surface.

compared to r_p,

$$a = \sqrt{2 l_0 r_p}. \quad [4]$$

Adhesion force and torque. Knowing the radius of the contact area, the adhesion force and torque are estimated following the assumptions of Hammer and Lauffenburger (40) and Kuo *et al*. (41): the bond density (i.e., concentration per unit area) is uniform in the contact area, the bonds can be modeled as Hookean springs, which are equally stressed, and the contribution of the nonspecific interactions (i.e., Van der Waals, double layer, and structural interactions (42, 43)) to the adhesion force is negligible. The most critical assumption is to suppose that the bonds are equally stressed. This is clearly an oversimplification (40), but has been previously implemented with success to predict trends that have been born out in model experimental systems for receptor/ligand interactions studies (19, 20). In contrast, the first assumption is quite reasonable in regards to the immobilization procedure, and the later assumption will be justified *a posteriori* by the experimental results.

In addition we assume that the fibrin bonds are parallel as the contact area radius is small compared to the particle radius (see Fig. 2). Thus, taking unitary vectors **i**, **j**, and **k** defined in Fig. 3, the adhesion force can be written as

$$\mathbf{F}_{\mathrm{Adh}} = -[\pi a^2 \mathcal{C} \sigma \lambda](\cos\alpha \mathbf{i} + \sin\alpha \mathbf{k}), \quad [5]$$

where $\mathcal{C}$ is the fibrin bonds density, σ is the spring stiffness, λ is

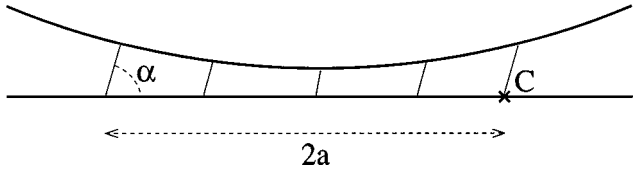

FIG. 2. Schematic diagram (not to scale) of the contact area between a particle and the flat surface. C defines the front edge of the contact area and α the angle between individual bonds and the flat surface.

the spring elongation, and α defines the direction of the bonds (see Fig. 2). The torque at the front edge of the contact area is

$$\mathbf{\Gamma}_{\mathrm{Adh_c}} = -\int_0^{2\pi}\int_0^{a} [\mathcal{C}\sigma\lambda\sin(\alpha)(a - r\cos\theta)] r\, dr\, d\theta \mathbf{j}, \quad [6]$$

where θ and r are the angular and radial coordinates in the contact area. This equation leads to

$$\mathbf{\Gamma}_{\mathrm{Adh_c}} = [\mathbf{F}_{\mathrm{Adh}} \cdot \mathbf{k} a]\, \mathbf{j}. \quad [7]$$

Thus, the collective behavior of the bonds is equivalent to the behavior of a single spring attached to the center of the contact area. The corresponding elongation is λ and the stiffness σ_{eq} is given by

$$\sigma_{\mathrm{eq}} = \pi a^2 \mathcal{C}\sigma = 2\pi l_0 r_p \mathcal{C}\sigma. \quad [8]$$

Hydrodynamic loads. In the ideal case of a laminar infinite linear shear flow over a single spherical particle in contact with an infinite plane wall at rest, the hydrodynamic drag (**D**), torque at sphere center ($\mathbf{\Gamma}_0$), and lift (**L**) are given by (44, 45)

$$\mathbf{D} = \left[32.0 r_p^2 \tau_w + \mathcal{O}(\mathrm{Re}_p)\right] \mathbf{i}, \quad [9]$$

$$\mathbf{\Gamma}_0 = \left[11.9 r_p^3 \tau_w + \mathcal{O}(\mathrm{Re}_p)\right] \mathbf{j}, \quad [10]$$

and

$$\mathbf{L} = 9.257 r_p^2 \tau_w \mathrm{Re}_p \mathbf{k}. \quad [11]$$

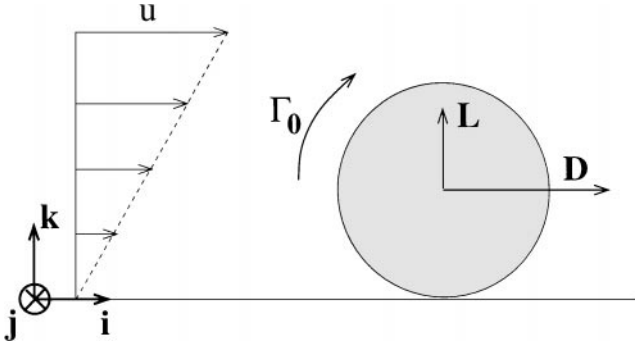

FIG. 3. Definition of unitary vectors and hydrodynamic loads exerted over a single particle. **D**, drag; $\mathbf{\Gamma}_0$, torque at sphere center; **L**, lift.

TABLE 2

Order of Magnitude of the Hydrodynamic Parameters in the Parallelepipedic Flow Channel and of Loads Exerted on an Isolated Particle Resting on the Channel Bottom

Flow rate (ml/min)	1	10	160	240
Shear stress (Pa)	0.25	2.5	40	60
Reynolds number Re_h	0.83	8.33	133	200
Entry length (mm)	0.02	0.22	3.64	5.46
Particular Reynolds number Re_p	0.00025	0.0025	0.04	0.06
Drag (pN)	8	80	1280	1920
Lift (pN)	0.0006	0.06	14.8	33.3
Drag/Lift	13827	1382	86	58
Torque (pN·μm)	2.98	29.8	476	714

Note. These values are calculated from $h = 0.1$ mm, $l = 5$ mm, $\mu = 1$ cP, $\nu = 10^{-6}$ m^2 s^{-1} and $r_p = 1$ μm, using Eqs. [1], [2], [9], [10], and [11].

In these expressions, Re_p denotes the particulate Reynolds number given by

$$Re_p = \frac{u(r_p)r_p}{\nu} = \frac{r_p^2\tau_w}{\nu\mu}, \quad [12]$$

where ν is the kinematic viscosity and $u(r_p)$ is the velocity of the undisturbed fluid at the center of the particle, and $\mathcal{O}(Re_p)$ are terms of order Re_p. For convenience, the velocity of the fluid at the particle center was replaced by $\frac{r_p \cdot \tau_w}{\mu}$, assuming a linear velocity profile close to the wall as r_p is negligible compared to h.

In the case of the three-dimensional laminar flow past an array of uniformly distributed spheres that are adherent to the bottom plate of a parallel plate flow channel, Eqs. [9], [10], and [11] still hold at less than 1% if the ratio of r_p to the gap thickness between parallel plates is less than $1/15$ and if the interparticular distance is greater than $5r_p$ (35). Both conditions are fulfilled in our experiments.

In addition, whatever the imposed flow rate, the flow is laminar (i.e., Re_h is small compared to 1000 (46)), Re_p is small compared to 1 and the length L_e of the entry region is small compared to the length of the rectangular flow channel (see Table 2). Therefore, the hydrodynamics loads acting on an individual particle at rest on the channel bottom may be calculated using Eqs. [9], [10], and [11]. Their order of magnitude is displayed in Table 2. In addition, the ratio between drag and lift is large. Lift may thus be neglected compared to drag in the detachment process.

Balance of forces and torques. Writing the equations of mechanical equilibrium of a particle leads to (a) force balance projected over **i**,

$$(\mathbf{F}_{Adh} + \mathbf{D}) \cdot \mathbf{i} = 0, \quad [13]$$

and (b) torque balance at the front edge of the contact area projected over **j**,

$$\mathbf{\Gamma}_{Adh_c} \cdot \mathbf{j} + \mathbf{\Gamma}_0 \cdot \mathbf{j} + r_p \mathbf{D} \cdot \mathbf{i} = 0. \quad [14]$$

From Eqs. [4], [5], [7], [9], and [11], we have

$$2\pi l_0 \mathcal{C}\sigma\lambda \cos\,\alpha = 32.0 r_p \tau_w \quad [15]$$

and

$$a2\pi l_0 \mathcal{C}\sigma\lambda \sin\,\alpha = 43.9 r_p^2 \tau_w. \quad [16]$$

Eliminating α between these two relationships leads to

$$\tau_w = \frac{\pi \mathcal{C}\sigma\lambda l_0}{r_p\sqrt{256 + 240\frac{r_p}{l_0}}}. \quad [17]$$

The relationship between adhesion force and shear stress at detachment τ_{det} is obtained, assuming that detachment occurs when the elongation of bonds equals the maximum elongation λ_{max} above which bonds rupture and that the particle still is in mechanical equilibrium. Thus,

$$\tau_{det} = \frac{\pi \mathcal{C}\sigma\lambda_{max} l_0}{r_p\sqrt{256 + 240\frac{r_p}{l_0}}}. \quad [18]$$

2.2.2. Analysis of Detachment Mechanism

The above relationship is valid whatever the detachment meachanism (sliding, rolling, or most probably sliding and rolling). However, it does not allow us to analyze the detachment mechanism, which is related to the value of α at detachment. In fact α tends toward $\frac{\pi}{2}$ when the detachment implies pure rolling and toward 0 when it implies pure sliding, as displayed in Fig. 4.

Using Eq. [15] and [16],

$$\frac{\cos\alpha}{\sin\alpha} = 1.03\sqrt{\frac{l_0}{r_p}}. \quad [19]$$

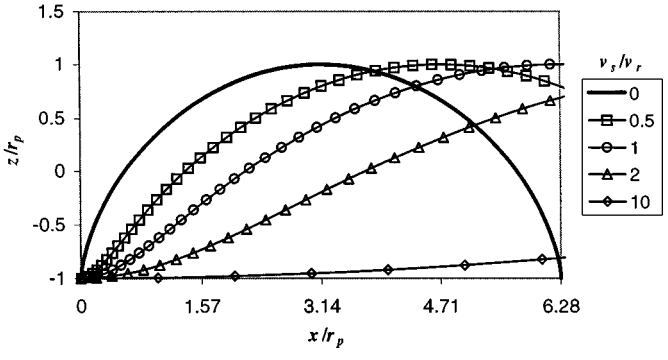

FIG. 4. Trajectory of the point on the particle corresponding initially to the center of the contact area during particle removal, for different ratios between sliding and rolling velocity. Detachment occurs when the distance between this point and the initial position of the center of the contact area equals λ_{max}. As λ_{max} is small compared to r_p, the value of α at detachment may be approximated by the origin tangent of the trajectory.

As l_0 is small compared to r_p, α is close to $\frac{\pi}{2}$ and the detachment should mainly imply rolling. By analogy with the dry rolling theory (47), we thus introduce the rolling friction coefficient g_0 whose dimension is a length, such as

$$|\mathbf{\Gamma}_0 + r_p[\mathbf{D}\cdot\mathbf{i}]\,\mathbf{j}| \le g_0\mathbf{F}_{Adh}\cdot\mathbf{k}, \qquad [20]$$

the equality of left and right terms being obtained at rupture. The rolling friction coefficient has been evaluated by Hubbe (37) as the radius of the contact area a. Using Eqs. [4], [5], [9] and [10], we obtain here

$$g_0 = \frac{21.9}{\sqrt{\frac{256}{r_p^2} + \frac{480}{a^2}}}, \qquad [21]$$

which is exactly a if we assume that $r_p \gg a$, which is the case in the present problem.

2.2.3. Effect of Particle Size Dispersion

In the case of an ideal population in which each particle is of the same radius and submitted to the same adhesive interactions, Eq. [18] implies that shear stress at detachment τ_{det} ought to be the same for each particle. Thus, the percentage of particles detached ought to be equal to zero for shear stresses ranging from 0 to τ_{det} and to be equal to 100% for higher shear stresses, displaying a sharp detachment curve. However, the particle population used in our experiments is not ideal. In particular, particle size distribution $\mathcal{N}(r_p)$, as measured by laser granulometry (Malvern Mastersizer, Malvern, UK), is Gaussian. Thus, the number of adherent particles as a function of the applied wall shear stress can be written as

$$N(\tau_w) = \int_{-\infty}^{r_p(\tau_w)} \mathcal{N}(r)\,dr, \qquad [22]$$

where $r_p(\tau_w)$ is the radius of particles detached by a shear stress equal to τ_w obtained by inversion of Eq. [18]. As Gaussian distributions are symmetric around the mean value, the wall shear stress that causes 50% particle detachment, denoted $\tau_{w\,50\%}$, is independent of the standard deviation of the distribution. In fact, $\tau_{w50\%}$ is the wall shear stress necessary to detach particles whose radius is equal to the mean radius of the distribution. Assuming that distributions of all other parameters implied in particles/surface interaction are symmetric, the wall shear stress that causes 50% particle detachment, widely used throughout the literature without further justification (19, 33, 37, 38), is thus a pertinent parameter for describing the interaction strength.

3. RESULTS AND DISCUSSION

In order to separate the nonspecific DLVO interactions from the specific fibrin/fibrin interactions implied in fibrin-coated particle adhesion to a fibrin-coated glass plate, preliminary experiments have been performed with amine or fibrin-coated latex particles in contact with clean glass. Then, in order to study fibrin/fibrin-specific interactions, three different particle/substrate systems have been investigated: fibrin-coated latex particles in contact with a fibrin monolayer (FM system), fibrin-coated latex particles in contact with a fibrin bilayer (FB system), and fibrin-coated latex particles in contact with a fibrin bilayer in presence of plasmin (PDFB system). For convenience, the results of all the detachment experiments have been classically plotted as the percentage of particles remaining attached to the substrate as a function of the wall shear stress applied. These results have been interpreted in terms of elastic force at rupture of an elementary intermonomeric fibrin bond, using the theoretical model proposed in the previous chapter.

3.1. Nonspecific Interactions

Results of the preliminary experiments performed using amine latex particles in contact with clean glass have been fitted using the function

$$N/N_0 = \exp\left(\frac{-\tau_w^{c_2}}{c_1}\right), \qquad [23]$$

where N/N_0 is the number of particles remaining in the observation area normalized by the initial deposited number, and c_1 and c_2 are two positive coefficients. For all the experiments ($n = 15$), the regression coefficient obtained was greater than 0.98. c_1 and c_2 were respectively between 0.47 and 1.47 and 0.5 and 1. $\tau_{w\,50\%}$ was then calculated using

$$\tau_{w\,50\%} = (-c_1 \ln(0.5))^{1/c_2} \qquad [24]$$

as 0.43 ± 0.25 Pa. The large variability of these results, demonstrated by the high standard deviation, was caused by noncontrollable external factors such as vibrations and noises, which have an important influence under conditions of weak adhesion.

The effects of ionic strength and pH on the adhesion of amine latex particles in contact with clean glass have been studied using IS Buffer (sodium phosphate 0.005 M, pH 7.4, NaCl 0.008 M, NaN_3 0.01%) and pH buffer (sodium phosphate 0.05 M, pH 9, NaCl 0.08 M, NaN_3 0.01%), respectively, instead of detachment buffer. $\tau_{w\,50\%}$ was calculated as described above as 0.09 ± 0.07 Pa ($n = 8$) and 0.38 ± 0.2 Pa ($n = 5$), respectively. The results, displayed in Fig. 5, were in good agreement with the DLVO theory, which describes the energy of interaction between two charged surfaces in a polar medium, as previously found by Elzo *et al.* (33). According to the classical DLVO theory the net energy of interaction is the summation of the attractive Van der Waals energy and the repulsive electric double-layer energy. Decreasing ionic strength increases the double-layer thickness, which results in higher repulsion and then in significantly weaker adhesion, in accordance with the experimental results ($p = 10^{-4}$). The effect of pH is based on the variations of the zeta potential of particles and substrate. The absolute value of the zeta potential is lower at acid pH. Therefore the electric double-layer

repulsion is weaker, resulting in stronger adhesion at acid pH. However, as the effect of pH has been studied at high ionic strength in our experiments, the decrease of $\tau_{w\,50\%}$ from pH 7.4 to pH 9 was not significant ($p = 0.35$), probably because of the major effect on adhesion of the high value of the ionic strength, which compresses the electric double layer. Therefore the results of Fig. 5 are in good agreement with the DLVO theory, showing the validity of the experimental methodology adopted to study adhesion.

In order to check whether the presence of a fibrin monolayer coated on the particle has an influence on the nonspecific interactions, the behavior of fibrin-coated particles in contact with clean glass have been studied. $\tau_{w\,50\%}$ was calculated as described above as 0.48 ± 0.22 Pa ($n = 8$). This is not significantly different from the value obtained studying amine latex particles in contact with clean glass ($p = 0.34$). Thus, the existence of the fibrin layer on the particles has no influence on the nonspecific interactions.

3.2. Fibrin/Fibrin-Specific Interactions

Results of detachment experiments performed using fibrin-coated latex particles in contact with a fibrin monolayer (two independent sets of four or five experiments) or a fibrin bilayer (four independent sets of four or five experiments) are displayed in Fig. 6. First, as expected, the percentage of detached particles increases with the wall shear stress applied. Second, the percentage of detached particles under a given shear flow is drastically decreased when fibrin/fibrin interactions take place, compared with the case where only nonspecific DLVO forces exist. In particular, a wall shear stress threshold under which no particle removal occurs is evidenced. Its value, calculated as $\tau_{w\,1\%}$, the wall shear stress that causes 1% particle detachment, is 0.94 ± 0.57 Pa in the FM system. When only nonspecific DLVO forces exist, this wall shear stress induces the detachment of more than 80% of the particles. Thus, the contribution of the nonspecific interactions in the total adhesion is negligible and the high adhesion obtained in the presence of fibrin layers both on the particles and on the glass surfaces is mainly driven by specific interactions due to fibrin polymer bonds.[3] Third, the adhesion of fibrin-coated particles increases with the number of fibrin layers prepared on the glass plate. The drastic gap of the shear stress threshold $\tau_{w\,1\%}$ to 28 ± 36 Pa in the FB system illustrates the higher adhesion obtained with fibrin bilayers on the glass plate ($p = 0.005$). Moreover, a higher percentage of particles remains attached at the end of the experiments in the FB system than in the FM system, which also shows the higher adhesion in the FB system. In particular, in the FB system, more than 50% of the particles remained attached at the end of 88% of the experiments performed, whereas it happened only in 28% of the FM experiments. In such experiments, the maximal wall shear stress applied (i.e., 100 Pa) was too small to detach 50% of the particles, and the maximal value of 100 Pa was used as $\tau_{w\,50\%}$. Thus, values of $\tau_{w\,50\%}$ displayed in Fig. 7 and Table 3 are underestimated. However, they will be used in the next section to calculate an order of magnitude of $\sigma\lambda_{\max}$, the elastic force at rupture of an elementary intermonomeric fibrin bond, using the simple adhesion model presented in Section 2.2.

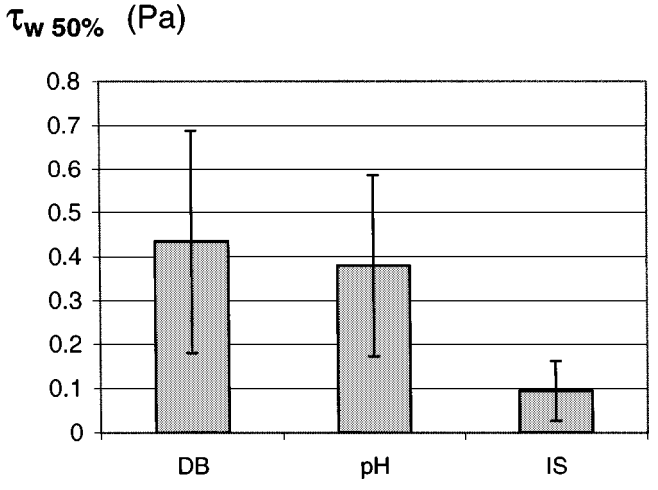

FIG. 5. Amine latex particles on clean glass: wall shear stress (mean and SD) allowing 50% particle detachment. DB, experiments performed with detachment buffer ($n = 15$); pH, experiments performed at higher pH (pH 9) with pH buffer ($n = 5$); IS, experiments performed at lower ionic strength (see text) with IS buffer ($n = 8$).

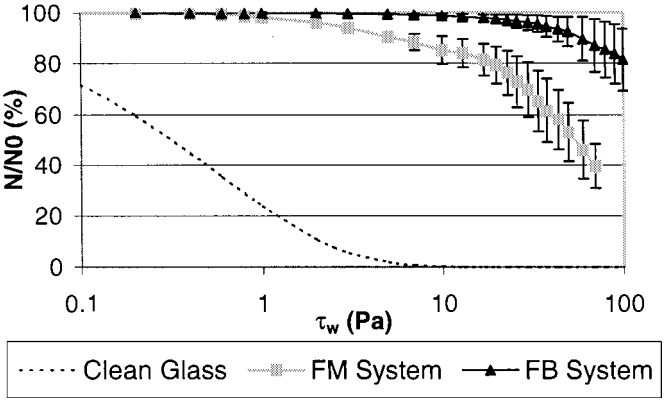

FIG. 6. Number of particles remaining in the observation area (expressed as a percentage of the initial number of particles) versus wall shear stress. Clean Glass, detachment of amine latex particles from clean glass (mean of the best fits using Eq. [23] of 15 experiments); FM System, detachment of fibrin-coated particles from a fibrin monolayer (two independent sets of four or five experiments); FB System, detachment of fibrin-coated particles from a fibrin bilayer (four independent sets of four or five experiments).

3.2.1. Elastic Force at Rupture of an Elementary Intermonomeric Fibrin Bond

As indicated by Eq. [18], the parameters governing the detachment of a particle are the fibrin bonds density $\mathcal{C}$, the characteristic thickness of the fibrin meshwork binding the particle

[3] This result offers the *a posteriori* justification for one of the assumptions used for estimating adhesion force and torque in Section 2.2.

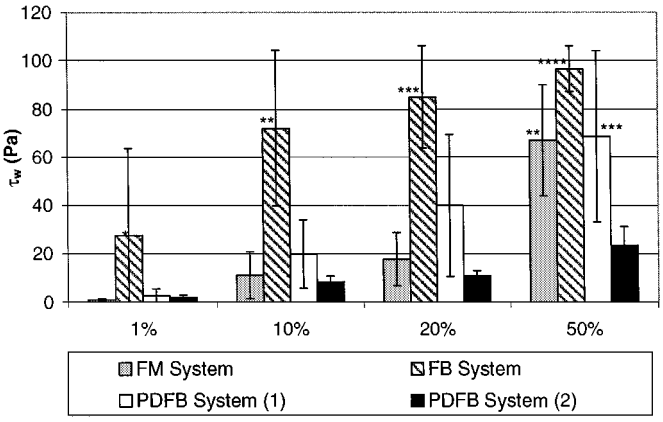

FIG. 7. Wall shear stress needed to detach 1, 10, 20, and 50% of initially deposed particles. FM System, detachment of fibrin-coated particles from a fibrin monolayer (two independent sets of four or five experiments); FB System, detachment of fibrin-coated particles from a fibrin bilayer (four independent sets of four or five experiments); PDFB System (1), detachment of fibrincoated particles from a plasmin-degraded fibrin bilayer (Set 1: five experiments); PDFB System (2), detachment of fibrin-coated particles from a plasmin-degraded fibrin bilayer (Set 2: five experiments). When the maximal wall shear stress applied at the end of the experiments (i.e., 100 Pa) was too small to detach the prescribed percentage of particles, the maximal value of 100 Pa was used. Thus, mean values displayed on this figure are underestimated. This underestimation increases with the percentage of experiments unable to detach the prescribed percentage of particles, as indicated by * symbols: *, between 10 and 20%; **, between 20 and 40%; ***, between 40 and 60%; ****, more than 80%.

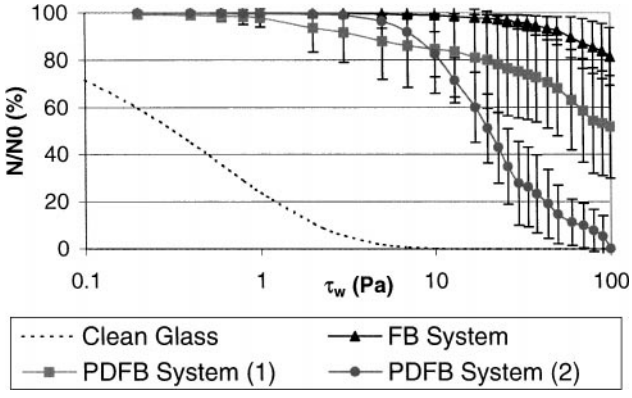

FIG. 8. Number of particles remaining in the observation area (expressed as a percentage of the initial number of particles) versus wall shear stress. Clean Glass, detachment of amine latex particles from clean glass (mean of the best fits using Eq. [23] of 15 experiments); FB System, detachment of fibrin-coated particles from a fibrin bilayer (four independent sets of four or five experiments); PDFB System (1), detachment of fibrin-coated particles from a plasmin-degraded fibrin bilayer (Set 1: five experiments); PDFB System (2), detachment of fibrin-coated particles from a plasmin-degraded fibrin bilayer (Set 2: five experiments).

to the flat surface l_0, the particle radius r_p, and the elastic force at rupture of an elementary intermonomeric fibrin bond $\sigma\lambda_{max}$. All of these parameters except $\sigma\lambda_{max}$ may be evaluated by independent methods. As determined by immunological characterizations, $\mathcal{C}$ is equal to $2460 \times 10^{12} \pm 20 \times 10^{12}$ bonds/m^2 (25). It can be assumed that l_0 is proportional to the total number of fibrin layers implied in binding the particle to the flat surface (two layers in the FM system, three layers in the FB system) and to the characteristic thickness of a fibrin monolayer, taken as the RMS roughness calculated from AFM measurements (i.e., 2.342 ± 0.551 nm). Finally, according to the manufacturer, r_p is equal to $1.05\ \mu\text{m} \pm 3.4\%$.

Thus, $\sigma\lambda_{max}$ may be calculated by Eq. [18] using these values and the experimentally determined $\tau_{w\,50\%}$. Results are reported in Table 3. The difference between $\sigma\lambda_{max}$ obtained in the FM and the FB systems is nonsignificant ($p = 0.1$). As the values of $\tau_{w\,50\%}$ displayed in Table 3 are underestimated (see above), this result must be taken carefully. However, it suggests that the elastic force at rupture of an elementary intermonomeric fibrin bond is an intrinsic quantity, independent of the number of fibrin layers implied in the adhesive contact.[4] Consequently, it suggests that the increased adhesion in the FB system compared to the FM system is mainly due to the increase in l_0, which in turn leads to an increase in the surface of the contact area.

Finally, the so-obtained value of $\sigma\lambda_{max}$ may be used to calculate the adhesion force. For example, in the FM system, F_{Adh} is about 35,000 pN (using Table 3 and Eq. [5]). Assuming that the separation distance is short compared to the sphere radius, the expression of the Van der Waals force for a sphere/plane system can be approximated as

$$F_{vdw} = \frac{A \cdot r_p}{6 \cdot d^2}, \qquad [25]$$

where A is the Hamaker constant (typically 10–20 J in water at 20°C) and d the separation distance (estimated as the surface roughness, i.e., l_0). The corresponding value of F_{vdw} is about 50 pN, confirming that the contribution of the Van der Waals force to the total adhesion force can be neglected.

TABLE 3

Calculation of the Elastic Force at Rupture of an Elementary Intermonomeric Fibrin Bond, from Experimental Results and Eq. [18] Using $\mathcal{C} = 2460 \times 10^{12}$ bonds/m^2, and $r_p = 1.05\ \mu$m

	$\tau_{w\,50\%}$ (Pa)	l_0 (nm)	$\sigma\lambda_{max}$ (pN)
FM system	67 ± 23	4.7	452 ± 155
FB system	97 ± 9	7.0	355 ± 34

3.2.2. Influence of Fibrin Degradation by Plasmin

Influence of fibrin degradation by plasmin is evidenced in Fig. 8, which displays the results of detachment experiments

[4] Note that the underestimation of the mean value of $\tau_{w\,50\%}$ is greater in the FB system than in the FM system, and that the corresponding value of $\sigma\lambda_{max}$ is smaller in the FB system than in the FM system, even if the absolute value of $\tau_{w\,50\%}$ is higher in the FB system. This is in favor of the independence of $\sigma\lambda_{max}$ of the number of fibrin layers implied in the adhesive contact.

performed using fibrin-coated latex particles in contact with a fibrin bilayer in the absence or presence of plasmin (four independent sets of four or five experiments and two independent sets of five experiments, respectively). Note that the results of the two independent sets of experiments performed in the presence of plasmin have been separately plotted, as they are significantly different. This difference may be explained by a different amount of fibrin degradation by plasmin, as suggested by the semi-quantitative immunological characterizations performed at the end of each experiment: in the first set, the increase of immunoreactivity of the monoclonal antibody DDi2F7 for fibrin-coated glass plates used in the detachment experiments compared to a control plate prepared simultaneously but not used in the detachment experiments was between 1.5 and 2, whereas it was between 4 and 10 in the second set. Thus, the amount of fibrin degradation was greater in the second set of experiments. This higher level of fibrin degradation induces a greater decrease in adhesion compared to the experiments performed in the absence of plasmin. First, as seen in Fig. 8, the final percentage of particles detached by the maximal wall shear stress applied (100 Pa) was $48 \pm 22\%$ in set 1 and $100 \pm 0\%$ in set 2. Second, $\tau_{w\,50\%}$ was reduced from 97 ± 9 Pa in absence of plasmin to 69 ± 35 Pa in set 1 ($p = 0.13$) and 23 ± 8 Pa in set 2 ($p = 2 \times 10^{-5}$). Finally, even in set 2 where the greater amount of fibrin was degraded, a shear stress threshold under which no particle is detached was evidenced (see Fig. 7).

Assuming that the lower adhesion observed in the presence of plasmin is only related to a decrease of the fibrin/fibrin bonds density due to fibrin degradation, and that the elastic force at rupture of the remaining nondigested fibrin/fibrin bonds as well as the characteristic thickness of a fibrin monolayer are unaffected, Eq. [18] may be used to estimate the fibrin/fibrin bonds density after plasmin degradation. Results are displayed in Table 4. They are in qualitative accordance with the semi-quantitative immunological controls performed at the end of each experiment.

In addition, the observed decrease in adhesion with increasing fibrin degradation not only demonstrates the influence of plasmin, but also supports the fact that the drastic increase in adhesion observed when fibrin is present on both particles and glass plate surfaces (compared to when one of the surfaces is bare) is really due to fibrin/fibrin-specific interactions rather than to the augmentation of surface roughnesses subsequent to fibrin immobilization.

TABLE 4

Calculation of the Effective Bond Density after Plasmin Degradation, from Experimental Results and Eq. [18], Using $\sigma\lambda_{max}$ = 355 pN, $\mathcal{C}_0 = 2460 \times 10^{12}$ bonds/m^2, and $r_p = 1.05\ \mu$m

	$\tau_{w\,50\%}$ (Pa)	l_0 (nm)	$\mathcal{C}$ (% $\mathcal{C}_0$)
FB system	97 ± 9	7.0	100 ± 9.7
PDFB system (set 1)	69 ± 35	7.0	71 ± 37
PDFB system (set 2)	23 ± 8	7.0	24 ± 8

4. CONCLUSION

The shear-induced detachment of spherical monodispersed fibrin-coated latex particles in adhesive contact with a plane fibrin-coated glass surface has been experimentally studied, focusing on the effect of the number of fibrin layers involved in the adhesive contact and of plasmin, the main physiological fibrinolytic enzyme. For that purpose, a shear stress flow chamber was carefully designed to generate a fully developed laminar two-dimensional Poiseuille flow, resulting in the accurate knowledge of hydrodynamic forces and torque acting on individual particles. In addition, the procedure for fibrin immobilization used a silane coupling agent associated with polyglutaraldehyde. Thus, in contrast to meshworks prepared by spraying or adsorption of fibrinogen (17, 11, 18), where immobilization of fibrinogen takes place by nonspecific physisorption resulting in conformational changes (48, 49), the conformation of fibrinogen was preseved as indicated by immunological studies (25, 29), and a firm attachment through covalent interactions was obtained. Stepwise preparation of fibrin layers resulted in the knowledge of the number of fibrin layers involved in the adhesive contact.

Qualitatively, it has been shown that (a) whatever the biochemical conditions of fibrin preparation and treatment (number of fibrin layers involved in the adhesive contact, absence or presence of plasmin), no particle removal occurs below a wall shear stress threshold, whose value $\tau_{w\,1\%}$ depends on these biochemical conditions, (b) over this shear stress threshold, increasing the wall shear stress causes an increase in particle detachment, and (c) the percentage of detached particles decreases with the number of fibrin layers involved in the adhesive contact and increases with plasmin degradation. In addition, the nonspecific DLVO interactions are negligible compared to the specific interactions between fibrin monomers.

Quantitatively, a simple adhesion model based on the balance of forces and torque on particles, assuming an elastic behavior of the fibrin polymer bonds, suggested that (a) the diminution of the percentage of detached particles with the number of fibrin layers involved in the adhesive contact should be related to the augmentation of the characteristic thickness of the fibrin meshwork binding the particle to the flat surface, which leads to an increase in the surface of the contact area, (b) the augmentation of the percentage of detached particles with plasmin degradation should be related to the diminution of the fibrin/fibrin bonds density, and (c) the experimental determination of the wall shear stress that causes 50% particle detachment allows the determination of the elastic force at rupture of an elementary intermonomeric fibrin bond. However, as in some experiments, the maximal wall shear stress generated by the shear stress flow chamber was too small to detach 50% of the particles. Our estimation of the elastic force at rupture of an elementary intermonomeric fibrin bond is only semi-quantitative, suggesting that this force (of order 400 pN) is an intrinsic quantity, independent of the number of fibrin layers involved in the adhesive contact. Further studies using larger particles could confirm or

infirm this hypothesis. If confirmed, the quantitative knowledge of the elastic force at rupture of an elementary intermonomeric fibrin bond could allow the theoretical study of the fragmentation of ensembles of particles connected by such elastic bonds and submitted to prescribed external loads. With regard to arterial thrombi fragmentation, such studies could be helpful to understand the relationship between the collective behavior of such ensembles and the mechanisms of removal of a single particle in contact with a flat substrate.

ACKNOWLEDGMENTS

We thank Dr. Houi, Dr. Marc-Vergnes, and Dr. Cassot for their active collaboration, Dr. Coratger for his expertise in AFM, and F. Esteban and S. Loyau for valuable technical assistance. Financial support from the INSERM (Intercommission 1 Grant 4M101C) and from the CNRS is gratefully acknowledged.

REFERENCES

1. Mosesson, M., *J. Lab. Clin. Med.* **116,** 8 (1990).
2. Kirchhofer, D., Tschopp, T., Steiner, B., and Baumgartner, H., *Blood* **86,** 3815 (1995).
3. Mosesson, M., *Nouvo Rev. Fr. Hematol.* **34,** 11 (1992).
4. Sakariassen, K., and Barstad, R., *Blood Coag. Fibrin.* **4,** 614 (1993).
5. Barstad, R., Kierulf, P., and Sakariassen, K., *Thromb. Haemostasis* **75,** 685 (1996).
6. Basmadjian, D., *J. Biomech.* **17,** 287 (1984).
7. Jobin, F., "La thrombose." Presses de l'Universit de Laval, Editions Maloine, Laval, 1995.
8. Sukavaneshvar, S., and Solen, K., *ASAIO J.* **44,** M388 (1998).
9. Barstad, R., Orvim, U., Hamers, M., Tjonnfjord, G., Brosstad, F., and Sakariassen, K., *Thromb. Haemostasis* **75,** 827 (1996).
10. Barstad, R., Roald, H., Cui, Y., Turitto, V., and Sakariassen, K., *Arterioscler. Thromb.* **14,** 1984 (1994).
11. Jirouskova, M., Dyr, E., Suttnar, J., Holada, K., and Trnkova, B., *Thromb. Haemostasis* **78,** 1125 (1997).
12. Orvim, U., Barstad, R., Stormorken, H., Brosstad, F., and Sakariassen, K., *Br. J. Haematol.* **95,** 389 (1996).
13. Sakariassen, K., Joss, R., Muggli, R., Kuhn, H., Tschopp, T., Sage, H., and Baumgartner, H., *Arteriosclerosis* **10,** 276 (1990).
14. Sakariassen, K., Aarts, P., De Groot, P., Houdijk, W., and Sixma, J., *J. Lab. Clin. Med.* **102** (1983).
15. Sukavaneshvar, S., Rossa, G., and Solen, K., *Ann. Biomed. Eng.* **28,** 182 (2000).
16. Graham, D., Huang, T., Keyt, B., and Alevriadou, R., *Ann. Biomed. Eng.* **26,** 712 (1998).
17. Jen, C., Li, H., Wang, J., Chen, H., and Usami, S., *Am. J. Physiol. (Heart. Circ. Physiol. 39)* **270,** H160 (1996).
18. Wu, Y., De Groot, P., and Sixma, J., *Arterioscler. Thromb. Vasc. Biol.* **117,** 3202 (1997).
19. Cozens-Roberts, C., Quinn, J., and Lauffenburger, D., *Biophys. J.* **58,** 107 (1990).
20. Kuo, S., and Lauffenburger, D., *Biophys. J.* **65,** 2191 (1993).
21. Kazal, L., Amsel, S., Miller, O., and Tocantins, L., *Proc. Soc. Exp. Biol. Med.* **113,** 989 (1963).
22. Grailhe, P., Boyer-Neumann, C., Haverkate, F., Grimbergen, J., Larrieu, M., and Anglés-Cano, E., *Blood Coag. Fibrin.* **4,** 679 (1993).
23. Blomback, B., and Blomback, M., *Ark Kemi.* **10,** 415 (1956).
24. Deutsch, D., and Mertz, E., *Science* **170,** 1095 (1970).
25. Anglés-Cano, E., *Anal. Biochem.* **153,** 201 (1986).
26. Wiman, B., and Wallen, P., *Eur. J. Biochem.* **36,** 25 (1973).
27. Ho Moon, J., Shin, J., Kim, S., and Park, J., *Langmuir* **12,** 4621 (1996).
28. Ikai, A., *Surf. Sci. Rep.* **26,** 261 (1996).
29. Fleury, V., and Anglés-Cano, E., *Biochemistry* **30,** 7630 (1991).
30. Bouhacina, T., Aime, J., Gauthier, S., and Michel, D., *Phys. Rev. B* **56,** 7694 (1997).
31. Drake, B., Prater, C., Weisenhorn, A., Gould, S., Albrecht, T., Quate, C., Cannell, D., Hansma, H., and Hansma, P., *Science* **243,** 1586 (1989).
32. Marchant, R., Barb, M., Shainoff, J., Eppel, S., Wilson, D., and Siedlecki, C., *Thromb. Haemostasis* **77,** 1048 (1997).
33. Elzo, D., Schmitz, P., Houi, D., and Joscelyne, S., *J. Membr. Sci.* **109,** 43 (1996).
34. Lorthois, S., Schmitz, P., Houi, D., and Anglés-Cano, E., *J. Adhes.* **72,** 229 (2000).
35. Brooks, S., and Tozeren, A., *Comp. Fluids* **25,** 741 (1996).
36. Pess, W., Teukolsky, S., Vetterling, W., and Flannery, B., "Numerical Recipes in C: The Art of Scientific Computing." Cambridge Univ. Press, Cambridge, UK. 1992.
37. Hubbe, M., *Colloids Surf.* **12,** 151 (1984).
38. Sharma, M., Chamoun, H., Sarma, S., and Schechter, R., *J. Colloid Interface Sci.* **149,** 121 (1992).
39. Yiantsios, S., and Karabelas, A., *J. Colloid Interface Sci.* **176,** 74 (1995).
40. Hammer, D., and Lauffenburger, D., *Biophys. J.* **52,** 475 (1987).
41. Kuo, S., Hammer, D., and Lauffenburger, D., *Biophys. J.* **73,** 517 (1997).
42. Elimelech, M., Gregory, J., Jia, X., and Williams, R., "Particle Deposition and Aggregation: Measurement, Modelling and Simulation." Butterworth Heinemann, Oxford, 1995.
43. Israelachvili, J., "Intermolecular and Surface Forces," Second ed. Academic Press, London, 1992.
44. O'Neill, M., *Chem. Eng. Sci.* **23,** 1293 (1968).
45. Krishnan, G., and Leighton, D., *Phys. Fluids* **7,** 2538 (1995).
46. Idel'cik, I., "Memento des pertes de charges: Coefficients de pertes de charge singulires et de perte de charge par frottement." Eyroles, Paris, 1986.
47. Gie, H., "Statique des solides et des fluides." J. P. Baillire et fils, Editeurs, Paris, 1964.
48. Retzinger, G., Cook, B., and Deanglis, A., *J. Colloid Interface Sci.* **168,** 514 (1994).
49. Sit, S , and Marchant, R., *Thromb. Haemostasis* **82,** 1053 (1999).